



Differential Diagnosis of Thick Myocardium according to Histologic Features Revealed by Multiparametric Cardiac Magnetic Resonance Imaging

Min Jae Cha¹, Cherry Kim², Chan Ho Park³, Yoo Jin Hong⁴, Jae Min Shin⁵, Tae Hoon Kim⁵, Yoon Jin Cha⁶, Chul Hwan Park⁵

¹Department of Radiology, Chung-Ang University Hospital, Seoul, Korea; ²Department of Radiology, Korea University Ansan Hospital, Ansan, Korea; ³Department of Radiology, Soonchunhyang University Cheonan Hospital, Cheonan, Korea; ⁴Department of Radiology and Research Institute of Radiological Science, Severance Hospital, Yonsei University College of Medicine, Seoul, Korea; ⁵Department of Radiology and Research Institute of Radiological Science, Gangnam Severance Hospital, Yonsei University College of Medicine, Seoul, Korea; ⁶Department of Pathology, Gangnam Severance Hospital, Yonsei University College of Medicine, Seoul, Korea

Left ventricular (LV) wall thickening, or LV hypertrophy (LVH), is common and occurs in diverse conditions including hypertrophic cardiomyopathy (HCM), hypertensive heart disease, aortic valve stenosis, lysosomal storage disorders, cardiac amyloidosis, mitochondrial cardiomyopathy, sarcoidosis and athlete's heart. Cardiac magnetic resonance (CMR) imaging provides various tissue contrasts and characteristics that reflect histological changes in the myocardium, such as cellular hypertrophy, cardiomyocyte disarray, interstitial fibrosis, extracellular accumulation of insoluble proteins, intracellular accumulation of fat, and intracellular vacuolar changes. Therefore, CMR imaging may be beneficial in establishing a differential diagnosis of LVH. Although various diseases share LV wall thickening as a common feature, the histologic changes that underscore each disease are distinct. This review focuses on CMR multiparametric myocardial analysis, which may provide clues for the differentiation of thickened myocardium based on the histologic features of HCM and its phenocopies.

Keywords: *Hypertrophy, left ventricular; Heart; Magnetic resonance imaging; Pathology; Histology; Diagnosis, differential*

INTRODUCTION

Left ventricular (LV) wall thickening or LV hypertrophy (LVH) is commonly observed in clinical practice [1]. Hypertrophic cardiomyopathy (HCM) is the most common genetic cardiomyopathy and is characterized by LVH

without an obvious cause [2,3]. However, various conditions, including hypertensive heart disease (HHD), aortic valve stenosis (AS), lysosomal storage disorders, cardiac amyloidosis, mitochondrial cardiomyopathy, sarcoidosis, and athlete's heart, should be considered as potential differential diagnoses [4,5]. The differential diagnosis of thickened myocardium can be challenging because these phenocopies share clinical features and morphological characteristics. Nevertheless, the pathophysiology and histological changes underlying these diseases are distinct [6-8].

Cardiac magnetic resonance (CMR) imaging may be a useful tool for establishing the differential diagnoses of various pathophysiologies based on histological changes in the myocardium. The heart is predominantly composed of cardiomyocytes, which are striated and have a well-ordered arrangement, and the extracellular interstitium, which comprises connective tissue that supports cardiomyocytes as a fibrous skeleton [9]. These ultrastructural features

Received: October 25, 2021 **Revised:** February 21, 2022

Accepted: February 27, 2022

Corresponding author: Yoon Jin Cha, MD, PhD, Department of Pathology, Gangnam Severance Hospital, Yonsei University College of Medicine, 211 Eonju-ro, Gangnam-gu, Seoul 06273, Korea.

• E-mail: yooncha@yuhs.ac; and

Chul Hwan Park, MD, PhD, Department of Radiology and Research Institute of Radiological Science, Gangnam Severance Hospital, Yonsei University College of Medicine, 211 Eonju-ro, Gangnam-gu, Seoul 06273, Korea.

• E-mail: park_chulhwan@yuhs.ac

This is an Open Access article distributed under the terms of the Creative Commons Attribution Non-Commercial License (<https://creativecommons.org/licenses/by-nc/4.0>) which permits unrestricted non-commercial use, distribution, and reproduction in any medium, provided the original work is properly cited.

of the heart constitute CMR features, including LV wall thickness, native T1 values, T2 values, and extracellular volume (ECV) fractions (Fig. 1). Various diseases characterized by LVH exhibit distinct histological features, such as cellular hypertrophy, cardiomyocyte disarray, interstitial fibrosis, extracellular accumulation of insoluble proteins, intracellular accumulation of fat, and intracellular vacuolar changes. These characteristics result in differential features in CMR multiparametric myocardial analysis and

characterization of myocardial tissue, which may facilitate differential diagnosis. The aim of this article was to discuss relevant CMR features for the differentiation of thickened myocardium, with an emphasis on the intrinsic histologic features of HCM and its phenocopies.

Hypertrophic Cardiomyopathy

HCM comprises a heterogeneous group of diseases

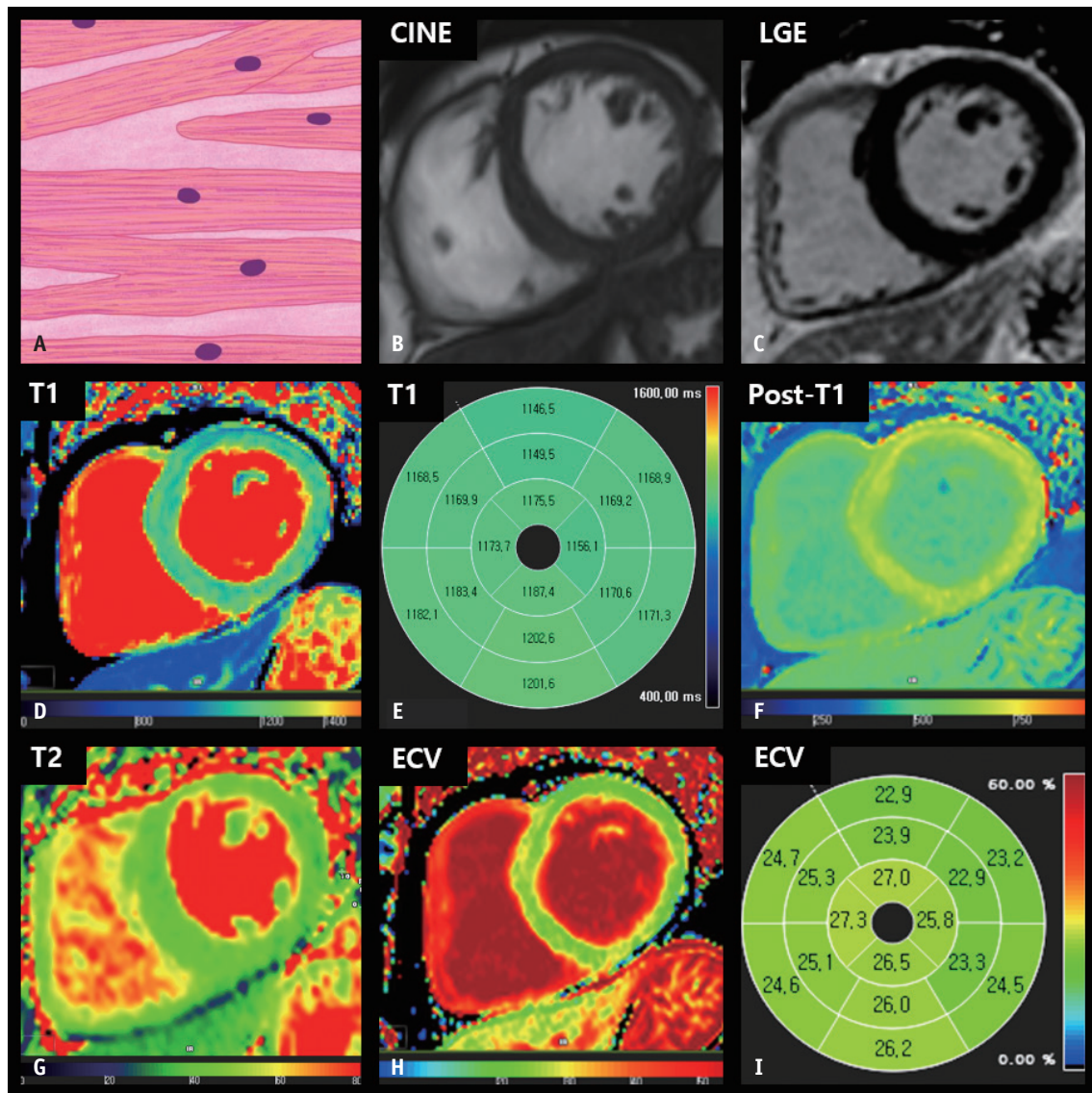


Fig. 1. CMR findings of normal LV myocardium based on histologic features.

A. A schematic illustration of representative histological findings of a normal heart shows that cardiomyocytes striate in a well-ordered arrangement, and extracellular connective tissue supports cardiomyocytes as a fibrous skeleton. The nuclei are centrally located and oval or fusiform in shape. **B.** The thickness of the LV myocardium is normally between 6 and 11 mm on cine images of the end-diastolic phase. **C.** The LV myocardium is homogeneously nulled and reveals a dark signal intensity on the LGE image. **D, E.** On native T1 maps, the LV myocardium generally exhibits homogeneous T1 values between 1174 and 1228 ms on 3T MRI. **F.** After contrast media injection, the myocardium reveals homogenous post-T1 values that are greater than those in the LV cavity. **G.** On T2 maps, normal myocardium usually demonstrates T2 values between 35 and 40 ms on 3T MRI. **H, I.** The ECV fraction of the LV is approximately 25%. CMR = cardiac magnetic resonance, ECV = extracellular volume, LGE = late gadolinium enhancement, LV = left ventricular

associated with sarcomere gene mutations, which are typically transmitted in an autosomal dominant pattern [3]. The natural disease course is diverse, ranging from no symptoms in mutation carriers to dyspnea, chest pain, syncope, and sudden cardiac death (SCD) [10,11]. Indeed, HCM is the most common cause of SCD in young individuals and athletes [12]. Thus, the accurate diagnosis of HCM is clinically significant. The diagnosis of HCM is generally based on imaging features. The asymmetric septal type is the most common morphological type of HCM [13]. The widely accepted diagnostic criteria for this type of HCM are LV end-diastolic wall thickness (EDWT) ≥ 15 mm or septal-to-lateral wall thickness ratio > 1.3 in the absence of LV chamber dilatation and other systemic diseases [14,15]. In apical HCM, myocardial thickening is confined to the LV apex and measures ≥ 15 mm, with an apical-to-basal LV wall thickness ratio of 1.3–1.5 [16,17]. Nevertheless, differentiation of HCM from its phenocopies based on myocardial thickness alone can be unreliable [18].

Histologically, the thickened myocardium in HCM exhibits structural abnormalities, including myofibrillary disarray, myocardial injury, replacement fibrosis, and an increase in interstitial connective tissue [16]. CMR imaging may facilitate the accurate diagnosis of HCM because of its ability to provide still images at end-diastole for precise measurement of myocardial thickness and because of its unique tissue characterization capabilities [19]. Conventionally, myocardial replacement fibrosis and scarring are identified using late gadolinium enhancement (LGE) imaging. Gadolinium contrast agents accumulate within the extracellular space in areas with scarring and are commonly described as patchy enhancements in the thickened myocardium [20–22]. However, almost half of patients with HCM have been reported to lack LGE on CMR imaging [23,24]. In such cases, multiparametric mapping techniques support the evaluation of distinct myocardial conditions. Patients with HCM exhibit increased native T1 and ECV fractions, reflecting the accumulation of interstitial fibrosis within an enlarged extracellular matrix. Prolonged T1 and elevated ECV fractions have been observed even in the absence of regional LGE and hemodynamic obstruction in HCM [25]. Patients with HCM may also exhibit an elevated native T2 value, which is associated with myocardial edema, inflammation, and increased risk of SCD [26,27]. In addition, strain imaging has provided evidence of myocardial disarray with decreased global longitudinal strain (GLS) parameters despite preservation of LV systolic

function (Fig. 2) [28].

Hypertensive Heart Disease

HHD arises due to systemic hypertension, and increased blood pressure accentuates hypertrophic remodeling via an increase in afterload and LV wall stress [29]. HHD typically manifests as concentric hypertrophy, absence of cardiac chamber dilatation, and LV wall thickness < 15 mm [30]. However, distinguishing HHD from HCM can be challenging if LV EDWT exceeds 15 mm [31] because HHD occurs as a result of pathological remodeling, similar to HCM [32]. One study reported that the segmental distribution of EDWT was not significantly different between the two groups [29]. LGE is more common in patients with HCM; however, half of the patients with HHD may exhibit LGE on CMR images. Although HCM more frequently presents as LGE at the right ventricular (RV) insertion point, LGE is less reliable for differentiating HHD from HCM [29,33,34]. Compared to those in normal controls, native T1 values and the ECV fraction are also increased in patients with HHD and LVH; therefore, these parameters are less useful for differentiating HHD from HCM (Fig. 3) [35].

Examination of histological changes may be useful for differential diagnosis. Histologically, HHD manifests as parallel alignment of hypertrophic cardiomyocytes [36]. In contrast, HCM presents with a disorganized arrangement of hypertrophic cardiomyocytes. Kato et al. [36] evaluated strain rates using tissue Doppler ultrasonography and reported that the septum/posterior wall thickness ratio was significantly higher in patients with HCM than in those with HHD, whereas the mean values of systolic strain were significantly higher in patients with HHD than in those with HCM. Notably, using these two parameters, that is, septum/posterior wall thickness ratio and systolic strain, HHD could be distinguished from HCM with 91% accuracy. Similarly, CMR imaging has been successfully applied for the differential diagnosis of HCM and HHD [29]. Puntmann et al. [34] reported that LV strain measured using cine images revealed that HCM was characterized by reduced global and regional deformation with preserved LV systolic function. In contrast, concentric LVH and relatively spared LV strain were suggestive of HHD rather than HCM. However, Neisius et al. [28] reported that there were no significant differences in strain parameters between HHD and HCM subgroups with equal LV wall thickness, although GLS was higher in patients with HHD. Accordingly, careful investigations that

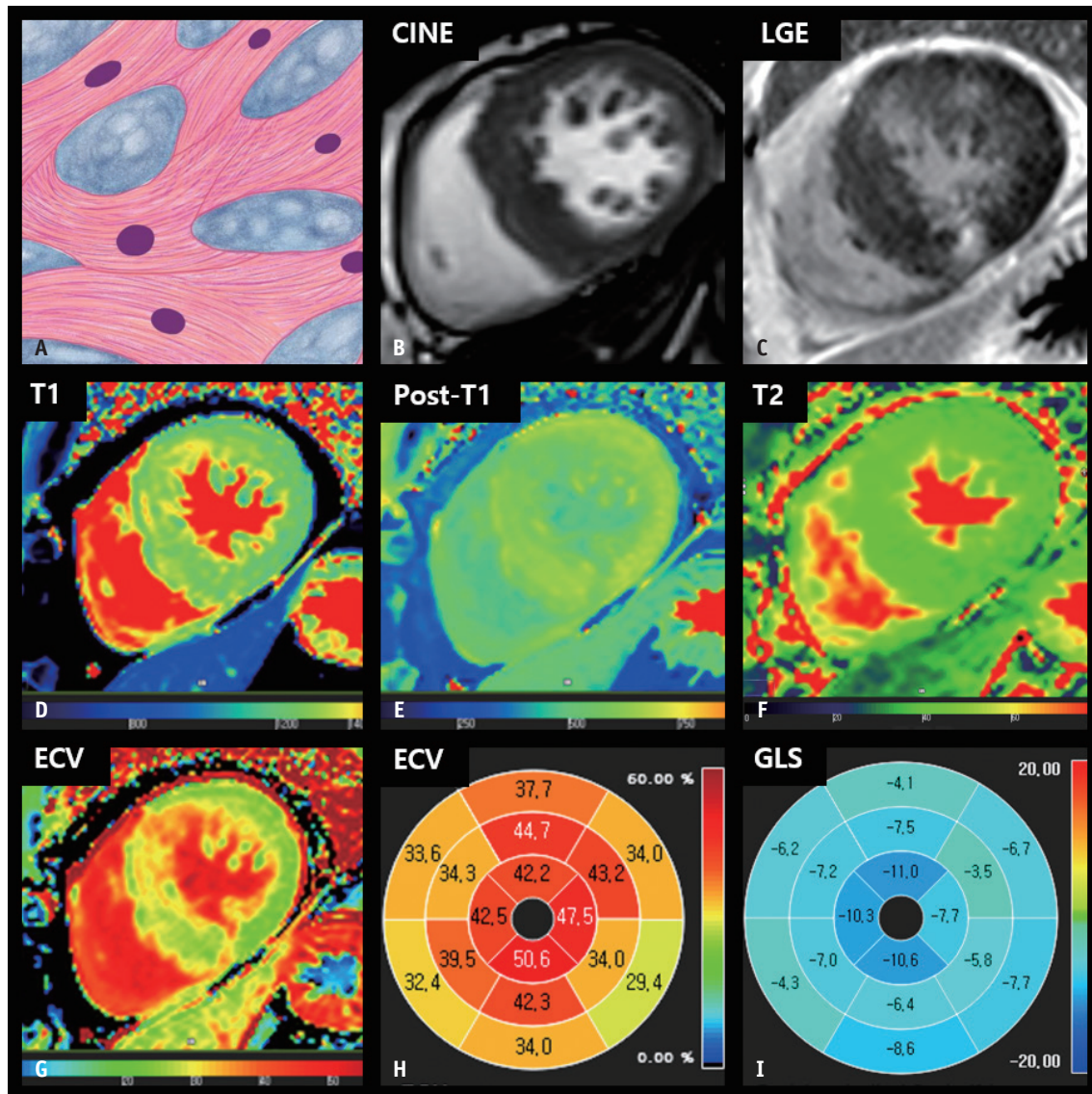


Fig. 2. CMR findings of HCM based on histologic features.

A. A schematic illustration of representative histological findings of HCM includes cardiomyocyte hypertrophy with a disorganized arrangement of fibers and interstitial fibrosis. Variations in muscle fiber thickness and enlarged and hyperchromatic nuclei are characteristic features. **B.** On short-axis cine images of the end-diastolic phase, the LV wall is thickened, measuring 18 mm. **C.** LGE imaging reveals patchy hyperenhancement in a thickened myocardium, which correlates histologically with regions of fibrosis. **D.** The native T1 map shows heterogeneous native T1 values of the myocardium, measuring up to 1320 ms on 3T MRI. **E.** After contrast media injection, the myocardium showed patchy areas with decreased post-T1 values. **F.** The T2 map shows increased T2 values of thickened myocardium, measuring up to 45 ms on 3T MRI. **G, H.** The ECV fraction map (**G**) and bull's eye diagram (**H**) demonstrate increased ECV of the myocardium, up to 50.6%. **I.** A bull's eye polar map of the GLS measured on cine images shows decreased absolute strain values in each myocardial segment. CMR = cardiac magnetic resonance, ECV = extracellular volume, GLS = global longitudinal strain, HCM = hypertrophic cardiomyopathy, LGE = late gadolinium enhancement, LV = left ventricular

consider the clinical scenario, multiparametric MR data, follow-up, and treatment responses are warranted to ensure an accurate diagnosis of HHD [18].

Aortic Valve Stenosis

AS is the most common valvular heart disease and can progress to afterload-induced heart failure [37,38]. LV

responses and adaptations to AS are heterogeneous, ranging from normal geometry to concentric, asymmetrical, and eccentric remodeling and hypertrophy [39]. LVH is a well-known sequela of chronic pressure overload due to AS, which is a compensatory mechanism for normalizing wall stress and maintaining cardiac output [40]. Asymmetrical LVH is fairly common and is observed in 27% of patients with AS [41]. Dweck et al. [39] reported that asymmetric

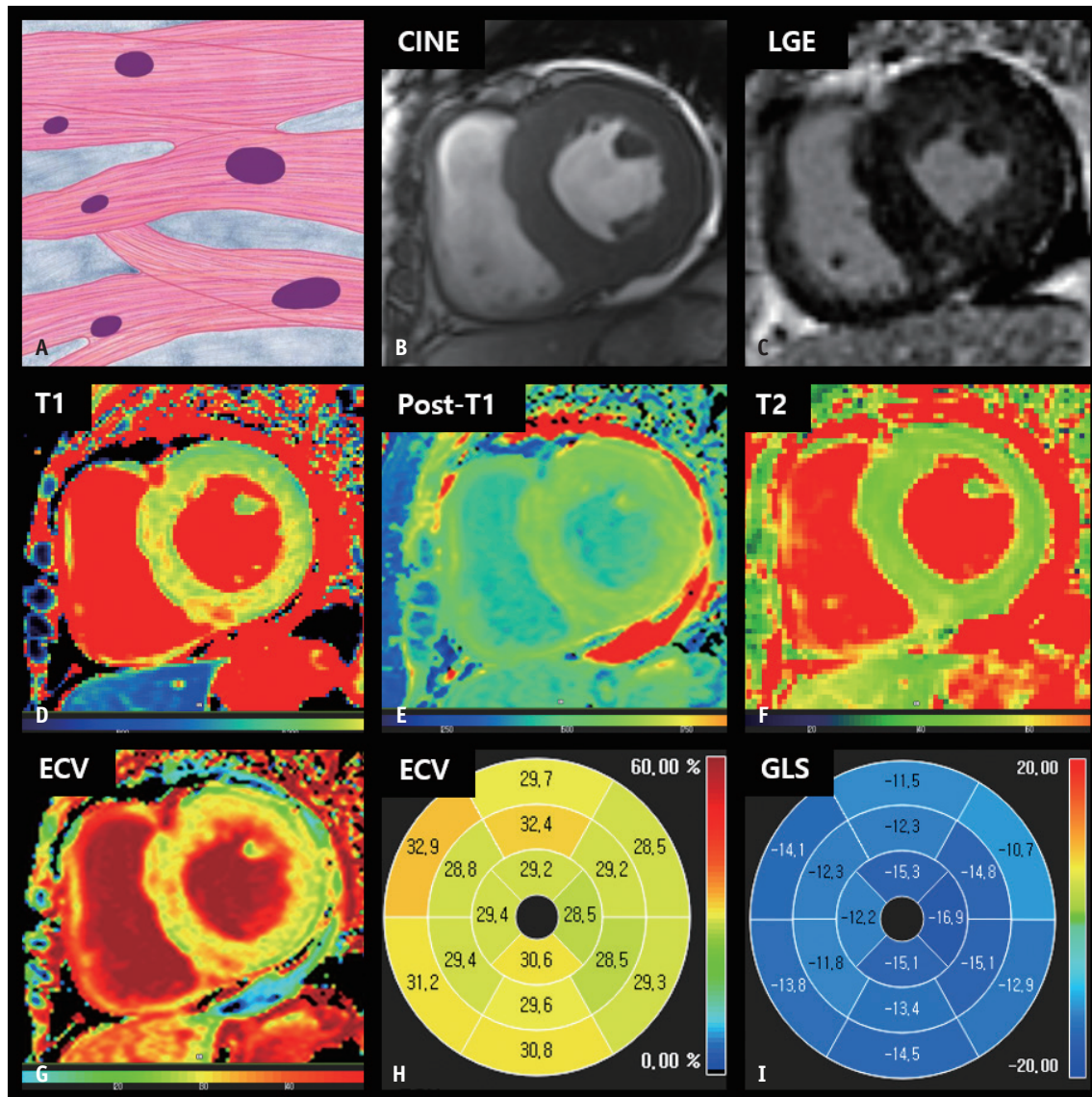


Fig. 3. CMR findings of hypertensive heart disease based on histologic features.

A. A schematic illustration of representative histological findings of hypertensive heart disease indicates that cardiomyocytes are hypertrophied with preserved parallel alignment. The intermuscular space is widened, and interstitial and perivascular fibrosis can be observed. **B.** On the short-axis cine image of the end-diastolic phase, the LV myocardium is concentrically thickened, measuring up to 17 mm. **C.** LGE image shows focal hyperenhancement at the right ventricular insertion points. **D.** The native T1 map shows slightly increased native T1 values of the LV septum, measuring up to 1286 ms on 3T MRI. **E.** On the post-contrast T1 map, the myocardium shows homogenous post-T1 values. **F.** The T2 map shows even T2 values. **G, H.** The ECV fraction map (**G**) and bull's eye diagram (**H**) demonstrate a slightly increased ECV fraction of the myocardium, up to 32.9%. **I.** A bull's eye polar map of the GLS measured on cine images shows relatively preserved LV strain values in each myocardial segment. CMR = cardiac magnetic resonance, ECV = extracellular volume, GLS = global longitudinal strain, LGE = late gadolinium enhancement, LV = left ventricular

LVH was most frequently observed in the basal-to-mid septum, with a mean thickness of 17 mm. Thus, HCM and AS may overlap considerably in morphological assessments.

Cardiac cine images may provide clues for the differential diagnosis of AS and HCM. Cine images show the systolic jet of turbulent flow across the aortic valve (AV), with a decreased AV area in AS. In contrast, in patients with HCM,

the jet is observed in the subaortic region, resulting from thickening of the adjacent basal LV anteroseptal wall [16]. LGE is less useful for differential diagnosis, as focal delayed hyperenhancement is a frequent finding on LGE imaging in patients with AS (Fig. 4) [42].

Characteristic histological features of AS include cardiomyocyte hypertrophy and extracellular matrix

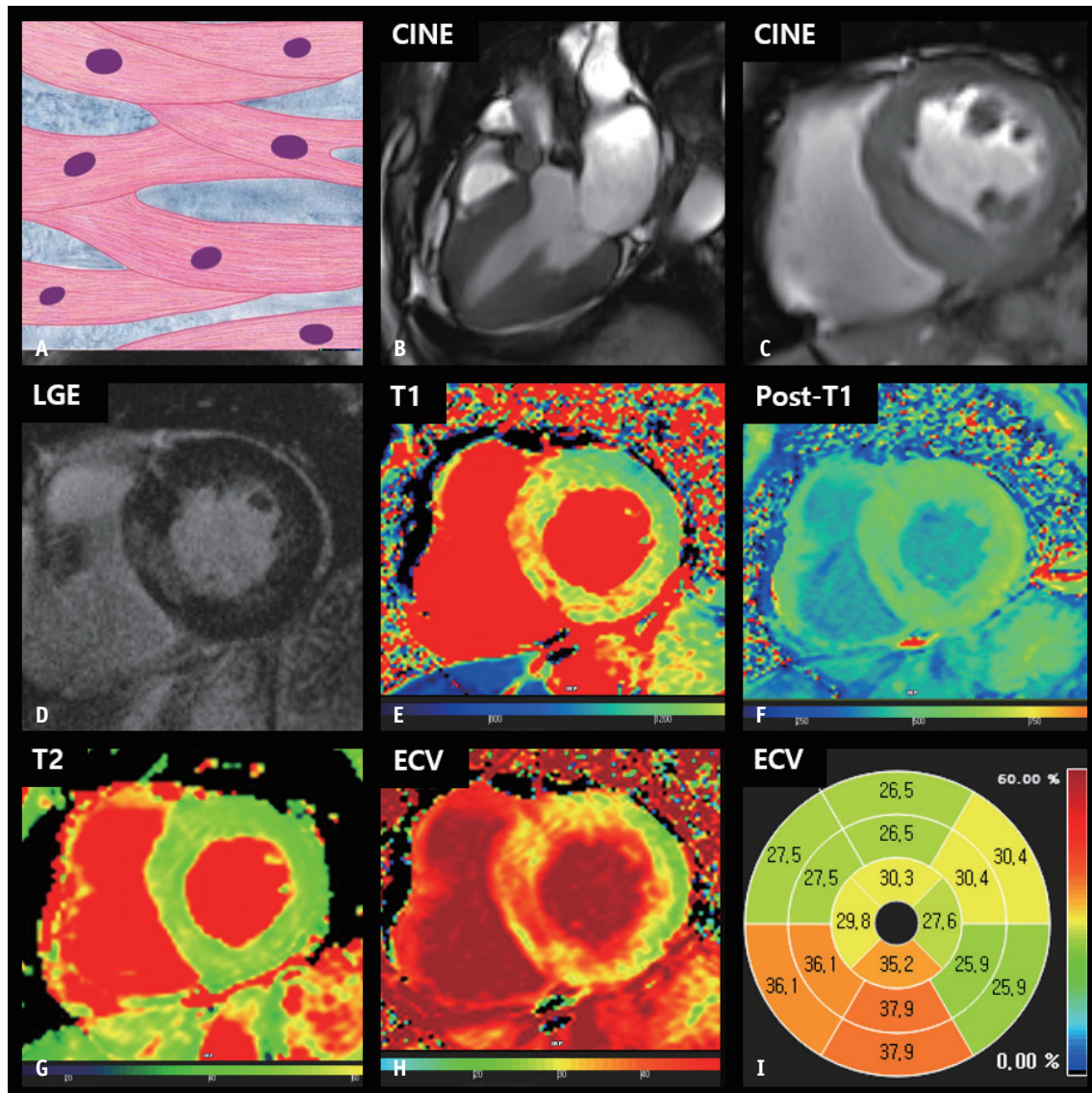


Fig. 4. CMR findings of aortic stenosis based on histologic features.

A. A schematic illustration of representative histological findings in aortic stenosis shows that cardiomyocytes are thickened and nuclei are enlarged with preserved muscle fiber alignment. **B.** Three-chamber cine image of the systolic phase shows thickened aortic valves with artifacts in the supra-valvular area. **C.** The left ventricular myocardium is concentrically thickened, measuring up to 18 mm on a short-axis cine image of the end-diastolic phase. **D.** LGE image reveals multifocal patchy myocardial scarring. **E.** The native T1 map shows increased native T1 values, measuring up to 1315 ms on 3T MRI. **F.** On the post-contrast T1 map, the myocardium shows heterogeneous post-T1 values with multifocal patchy foci and decreased T1 values. **G.** The T2 map shows relatively even myocardial T2 values. **H, I.** The ECV fraction map (**H**) and bull's eye diagram (**I**) demonstrate an increased ECV fraction in the myocardium. CMR = cardiac magnetic resonance, ECV = extracellular volume, LGE = late gadolinium enhancement

expansion with interstitial fibrosis, which eventually leads to cellular apoptosis and subsequent replacement fibrosis [43]. Studies have reported increased native T1 values and ECV fractions in patients with AS, but there may be a substantial overlap with normal control values [40,44]. However, a significant correlation between native T1 values and ECV fractions with AS severity, LV mass, and cardiac function in patients with AS has been reported

[44]. In addition, recent studies have demonstrated that ECV is a significant predictor of severe myocardial fibrosis and long-term clinical outcomes in patients with AS, highlighting the prognostic power of CMR markers [45-47]. Furthermore, CMR imaging provides additional insights into LV reverse remodeling after AV replacement. Studies have demonstrated that LV mass regression after surgery results from decreased interstitial fibrosis and regression of

cardiomyocyte hypertrophy, but focal replacement scarring and LGE do not resolve [45]. In terms of CMR strain analysis in patients with AS, research on the differentiation of AS from various HCM phenotypes using the CMR strain is limited. Instead, various CMR strain studies have focused on predicting myocardial remodeling in patients with AS. Hwang et al. [48] reported that LV GLS is associated with postoperative LV remodeling in patients with severe AS. Peak LV circumferential strains are also reportedly associated with postoperative mortality [49]. In addition, two-dimensional global longitudinal peak strain on CMR has been suggested as a prognostic predictor of clinical cardiac events in asymptomatic patients with AS and preserved cardiac function [50].

Liposomal Storage Disease

Anderson-Fabry disease (henceforth referred to as Fabry disease) is a rare genetic multisystem lysosomal storage disorder characterized by intracellular accumulation of glycosphingolipids caused by alpha-galactosidase A deficiency [51]. Cardiac involvement is important for prognosis and is reported in 40%–60% of patients with Fabry disease [52,53]. In cases of Fabry disease with cardiac involvement, ventricular (mainly LV) hypertrophy occurs, resulting in heart failure, valvular abnormality, ischemia, and arrhythmia [53]. Thus, CMR imaging may be a useful tool for the diagnosis of Fabry disease. On cine imaging, concentric LVH is common and the LV mass is increased. Diastolic dysfunction appears first and may be followed by a decrease in systolic function as myocardial fibrosis progresses [53,54]. For CMR strain analysis, Mathur et al. [55] demonstrated that the global longitudinal and circumferential strains from patients with Fabry disease did not differ significantly from those of healthy controls. Instead, they suggested that loss of the base-to-apex circumferential strain gradient might be an early marker of cardiac Fabry disease. On LGE imaging, inferolateral mesocardial distributed LGE is a well-established feature of Fabry disease [56].

A key feature in the differential diagnosis of Fabry disease is intracellular lipid accumulation with fat vacuoles [56]. Fat has a very short T1 value (usually 250 ms), and fat vacuoles shorten the T1 value of the myocardium. Therefore, T1 mapping is useful for diagnosing Fabry disease. Various heart diseases, including HHD, HCM, cardiac amyloidosis, sarcoidosis, and AS, exhibit increased values on T1

mapping. Low native T1 values in the septum are strongly suggestive of Fabry disease rather than HCM or other cardiac diseases with LVH [57,58]. Furthermore, T1 values of the interventricular septum can be used to evaluate cardiac involvement in Fabry disease without LVH and to monitor treatment responses [59–61]. The ECV fraction and T2 values may increase in the area of hyperenhancement on LGE imaging, suggesting myocardial fibrosis or inflammatory changes [59,62]. However, myocardium with a low native T1 value typically demonstrates normal ECV fraction and T2 values (Fig. 5).

Cardiac Amyloidosis

Amyloidosis comprises a group of diseases underscored by the extracellular deposition of amyloid fibrils, which are insoluble proteins formed by the breakdown of normal and/or abnormal proteins [63,64]. Cardiac amyloidosis is uncommon; however, cardiac involvement in amyloidosis results in progressive restrictive cardiomyopathy and is a major prognostic factor in patients with systemic amyloidosis [65,66]. Two main types of cardiac amyloidosis exist, immunoglobulin light-chain amyloidosis (AL) and transthyretin amyloidosis (ATTR). ATTR is divided into mutant (ATTRm) and wild-type (ATTRwt) forms according to the presence or absence of genetic mutations [67]. Early diagnosis of cardiac amyloidosis is essential for a better prognosis [68]. CMR imaging has been employed for diagnosing cardiac amyloidosis with excellent sensitivity and specificity [64]. On cine images, asymmetric or symmetric LV wall thickening is common [69,70] and can be accompanied by thickening of the RV or atrial wall [71]. Strain analysis using cine images could help in the early diagnosis, severity evaluation, and prognosis assessment of cardiac amyloidosis [65]. Decreased strain parameters with relative apical sparing are well-known characteristics of cardiac amyloidosis [72]. However, strain abnormalities are not specific for cardiac amyloidosis [65]. Diffuse annular LGE is a typical finding in amyloidosis. However, various types of abnormal LGE are possible, including focal patchy, diffuse patchy, subendocardial, subepicardial, and diffuse transmural or global LGE [65]. Therefore, the differential diagnosis of HHD, HCM, and other restrictive cardiomyopathies can be challenging.

The key histological feature of cardiac amyloidosis is the deposition of amyloid fibrils in the myocardial interstitium and edematous changes [65]. On quantitative mapping

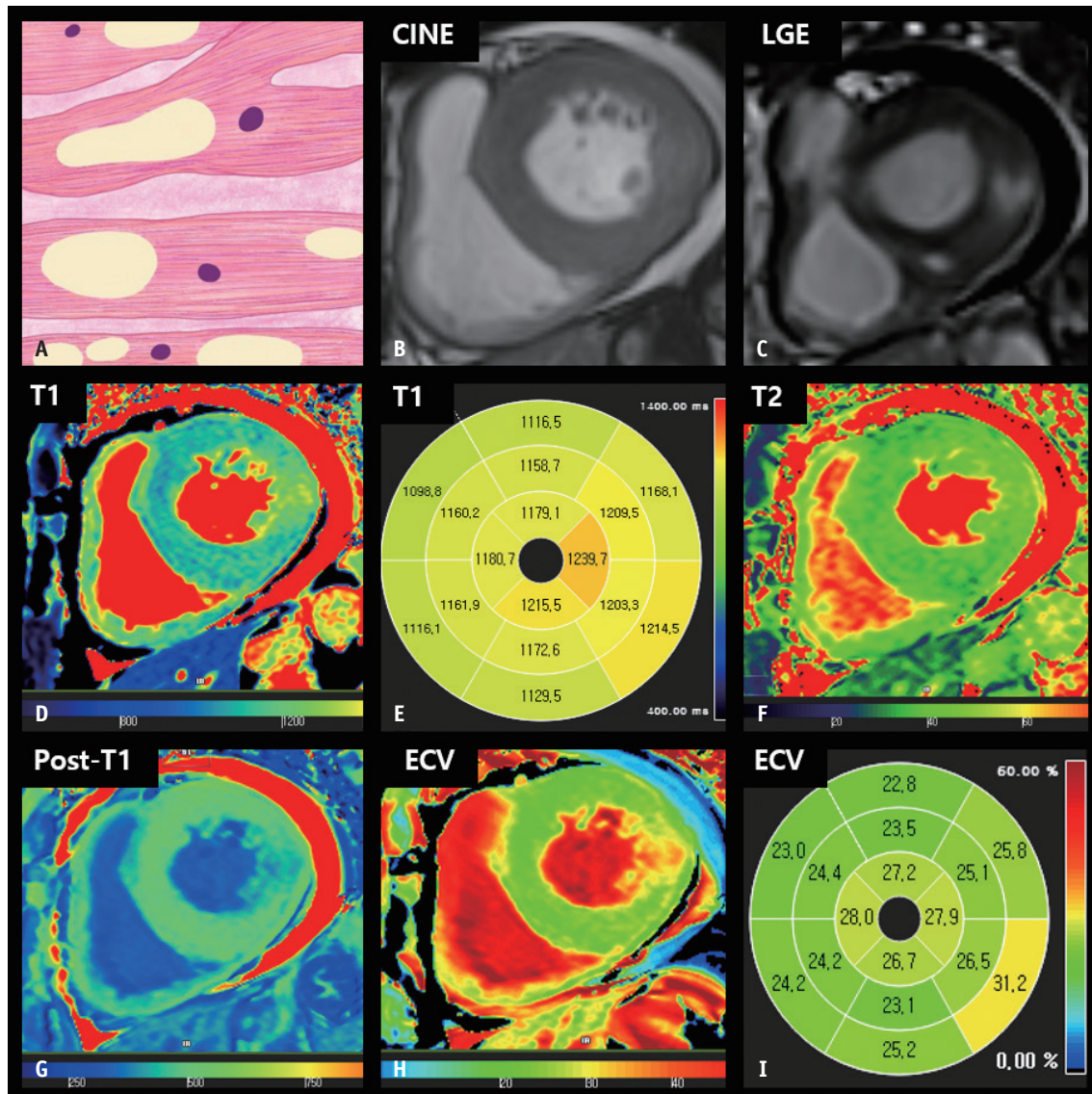


Fig. 5. CMR findings of Anderson-Fabry disease based on histologic features.

A. The distinct histological feature of Fabry disease is the accumulation of intracellular lysosomal glycosphingolipids. A schematic illustration of representative histologic findings revealing hypertrophic myocytes with perinuclear and cytoplasmic vacuoles. **B.** On the short-axis cine image of the end-diastolic phase, the LV wall showed concentric thickening. **C.** LGE imaging revealed focal hyperenhancement in the lateral free wall of the basal left ventricle. **D, E.** The native T1 map shows heterogeneous T1 values of the myocardium, with decreased native T1 values at the basal LV septum and increased native T1 values at the lateral free wall. **F.** The T2 map shows slightly increased T2 values at the lateral free wall. **G.** After contrast media injection, the myocardium demonstrated a focal area of decreased post-T1 values in the lateral LV wall. **H, I.** The ECV fraction map (**H**) and bull's eye diagram (**I**) show an increased ECV fraction at the lateral free wall, corresponding to the LGE area. CMR = cardiac magnetic resonance, ECV = extracellular volume, LGE = late gadolinium enhancement, LV = left ventricular

images, cardiac amyloidosis presents as high T1 values, high T2 values, and a high ECV fraction, representing myocardial edematous changes (T1 and T2 values) or amyloid burden (T1 values and ECV fraction) [65,73]. In particular, ECV is substantially higher in patients with amyloidosis than in those with other conditions that cause LVH (Fig. 6) [58]. Compared to amyloidosis, ATTR tends to exhibit more extensive and transmural LGE, a higher ECV fraction, and

lower T1 or T2 values, representing greater amyloid burden infiltration and less myocardial edema [64].

In addition, bone scintigraphy is useful for differentiating ATTR from AL. Bone scintigraphy using technetium 99m (^{99m}Tc) pyrophosphate, ^{99m}Tc-3,3-diphosphono-1,2-propanodicarboxylic acid, and ^{99m}Tc-hydroxymethylene diphosphonate revealed myocardial uptake of radiotracers with high sensitivity and specificity in patients with ATTR

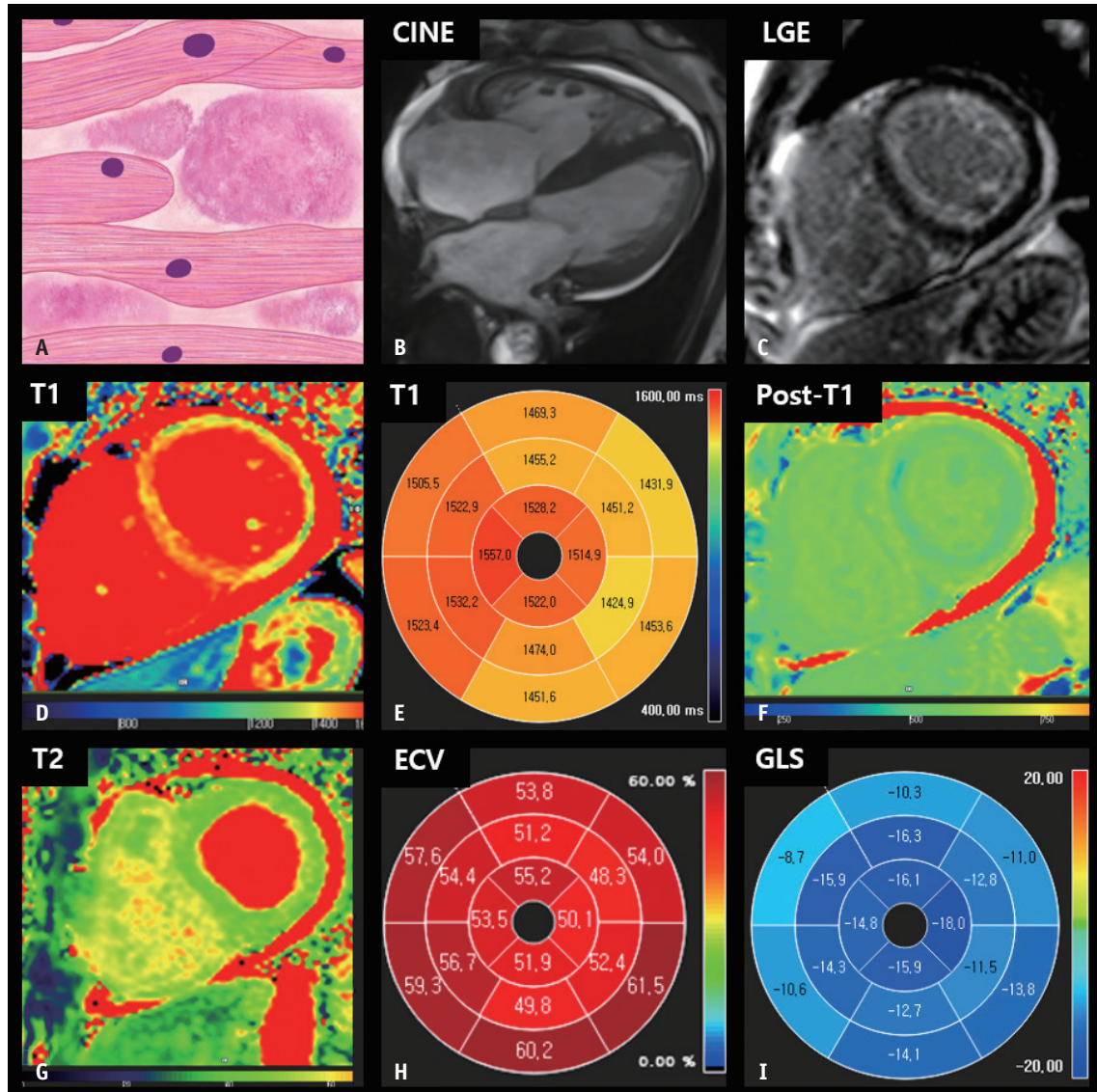


Fig. 6. CMR findings of immunoglobulin light-chain amyloidosis based on histologic features.

A. A schematic illustration of representative histologic findings of cardiac amyloidosis showing interstitial deposits of amorphous material (amyloid). **B.** In the four-chamber cine image of the end-diastolic phase, diffuse LV and right ventricular wall thickening are observed. **C.** LGE image reveals diffuse circumferential LV subendocardial hyperenhancement. **D, E.** The native T1 map shows diffusely increased native T1 values in the myocardium. **F.** After contrast media injection, the myocardium demonstrates low subendocardial post-T1 values in the left ventricle. **G.** The T2 map shows diffusely increased T2 values in the myocardium, measuring up to 55 ms. **H.** The bull's eye diagram of ECV fraction demonstrates a markedly increased ECV fraction of the myocardium, which is calculated to be up to 61.5%. **I.** A bull's eye polar map of the GLS measured on cine images shows decreased ventricular strain values with relative apical sparing. CMR = cardiac magnetic resonance, ECV = extracellular volume, GLS = global longitudinal strain, LGE = late gadolinium enhancement, LV = left ventricular

[74,75]. In contrast, patients with amyloidosis show no significant myocardial uptake [65].

Mitochondrial Cardiomyopathy

Mitochondrial myopathies are a heterogeneous group of disorders caused by mutations in the maternally inherited mitochondrial genome [76]. Mitochondrial myopathies

are associated with dysfunctional energy production and multisystemic involvement of the central nervous system, heart, and skeletal system. Mitochondrial myopathy-related cardiac abnormalities include dilated cardiomyopathy and HCM phenotypes. The HCM phenotype is the most common cardiac abnormality in patients with mitochondrial disease-related cardiomyopathy [77] and is typically characterized by concentric LVH [76]. When mitochondrial cardiomyopathy

presents as LVH, the differential diagnosis can be challenging [78], and the major role of cardiac imaging is to exclude other possible infiltrative or inflammatory diseases [79]. LGE images of patients with mitochondrial cardiomyopathies may exhibit non-coronary multifocal LGEs [79]. Perfusion MRI may indicate perfusion defects in LGEs [80] or subendocardial perfusion defects [79].

A key histological feature of mitochondrial cardiomyopathy is cardiomyocyte hypertrophy with vacuolar changes, derived from abnormal mitochondrial

accumulation, which appears as a red fiber on modified Gomori trichrome staining. An increased number of swollen mitochondria with variable sizes and shapes constitutes a distinct feature in electron microscopic evaluation [79]. Intracellular vacuolar changes indicate increased water content in the myocardium, resulting in a diffuse increase in the T2 signal or values in the LV myocardium (Fig. 7). In addition, concomitant hearing loss, low skeletal mass, and pericardial effusion are suggestive of mitochondrial cardiomyopathy [79].

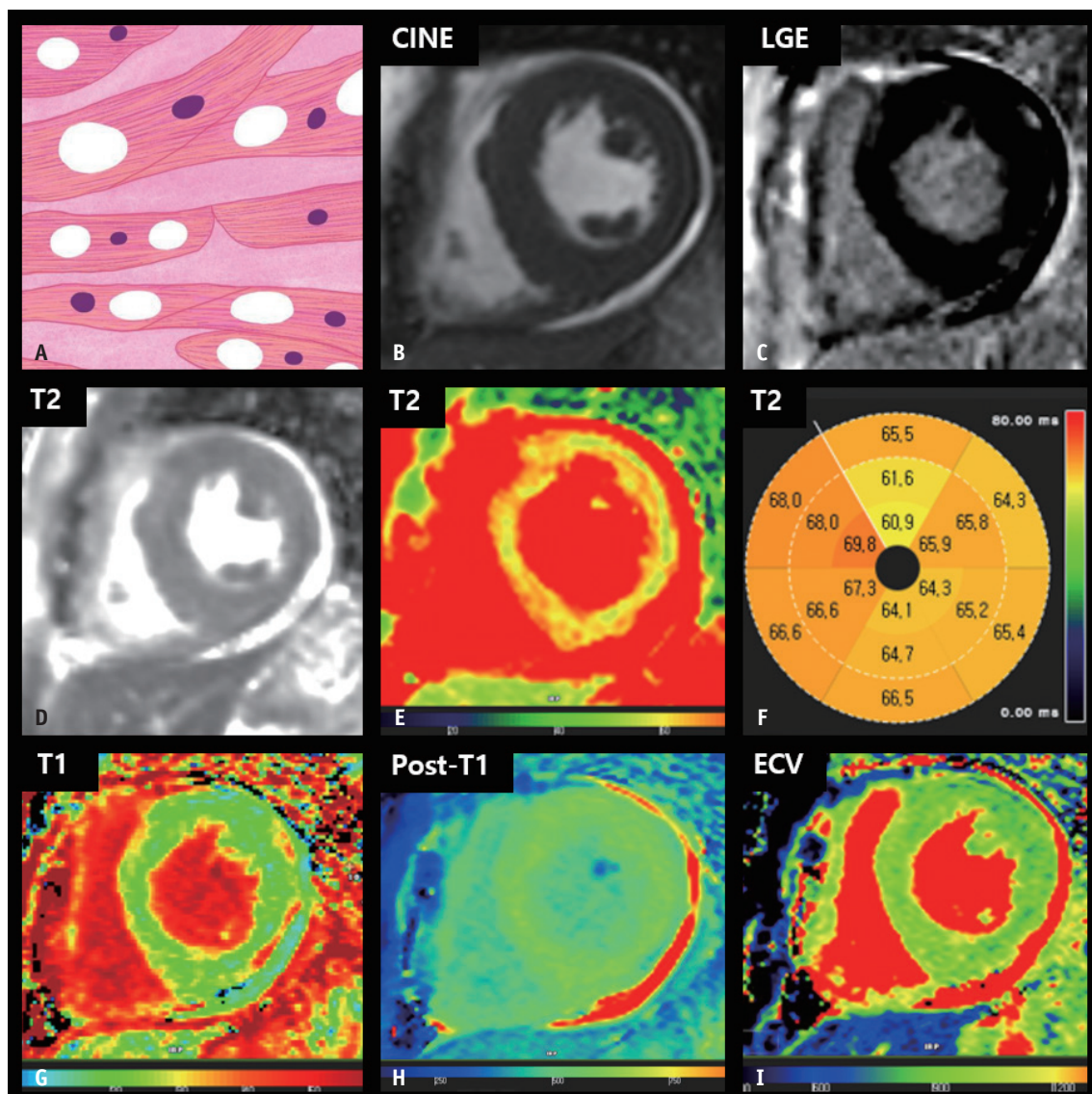


Fig. 7. CMR findings of mitochondrial cardiomyopathy based on histologic features.

A. A schematic illustration of the histological features of mitochondrial cardiomyopathy indicating myocyte hypertrophy with vacuolar changes. **B.** On short-axis cine image of the end-diastolic phase, the LV shows concentric wall thickening. **C.** LGE imaging reveals the absence of focal abnormal hyperenhancement in the LV. **D-F.** The T2 maps (**D, E**) and bull's eye diagram (**F**) show diffusely increased T2 values of the myocardium, measuring up to 69.8 ms on 1.5T MRI. **G.** The native T1 map shows diffusely increased native T1 values of the myocardium, measuring up to 1150 ms on 1.5T MRI. **H.** After contrast media injection, the myocardium reveals homogeneous post-T1 values in the LV. **I.** The ECV fraction map shows normal LV ECV fraction. CMR = cardiac magnetic resonance, ECV = extracellular volume, LGE = late gadolinium enhancement, LV = left ventricular

Sarcoidosis

Sarcoidosis is a multisystem disorder of unknown etiology. The histologic hallmark of sarcoidosis is the presence of non-caseating non-necrotic granulomas in the involved organs. The clinical manifestation of cardiac involvement occurs in approximately 5% of patients with sarcoidosis [81]. However, autopsy studies have estimated

that the prevalence of cardiac involvement in patients with sarcoidosis is at least 25% [82]. The major clinical manifestations of cardiac sarcoidosis include conduction abnormalities, ventricular arrhythmias, and heart failure [83]. Patients with cardiac involvement have a poorer prognosis than those without cardiac involvement [84]. Thus, timely and accurate diagnosis and management of cardiac sarcoidosis is critical.

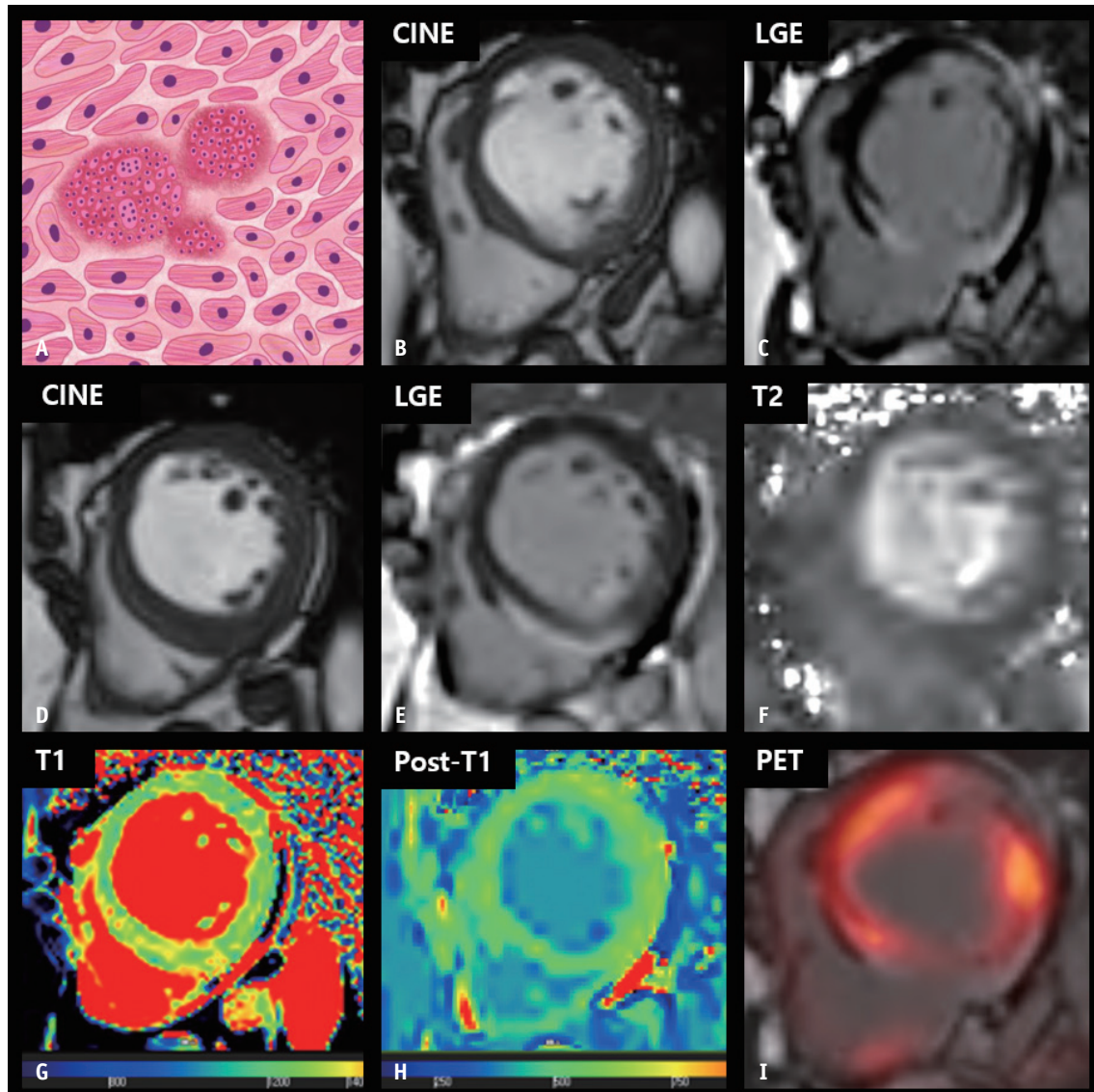


Fig. 8. CMR findings of cardiac sarcoidosis based on histologic features.

A. A schematic illustration of the histological features of sarcoidosis represents interstitial non-caseating granulomas, comprising a collection of epithelioid histiocytes and lymphocytes with multinucleated giant cells distributed along the lymphatics. **B, C.** On the short-axis cine image of the end-diastolic phase, basal thinning of the interventricular septum is noted (**B**), with epicardial or transmural enhancement on the LGE image (**C**). **D, E.** At the mid-left ventricular level, the interventricular septum shows mild thickening, measuring up to 16 mm (**D**), with hyperenhancement of the epicardial layer on the LGE image (**E**). **F.** The T2 map shows heterogeneously increased myocardial T2 values. **G.** The native T1 map shows increased native T1 values, measuring up to 1350 ms on 3T MRI. **H.** The post-T1 map demonstrates relatively lower post-T1 values at the epicardial layer of inferoseptal wall, corresponding to the LGE area. **I.** The LGE image of the basal level with fusion of ^{18}F -labeled fluoro-2-deoxyglucose PET suggests active inflammation surrounding the regions of an established scar. CMR = cardiac magnetic resonance, LGE = late gadolinium enhancement

A consensus statement on cardiac sarcoidosis by a consortium of international experts proposed LGE on CMR imaging as a criterion for the diagnosis of cardiac sarcoidosis [85]. The LGE pattern of cardiac sarcoidosis is patchy and multifocal with transmural involvement or sparing of the endocardial border; however, this pattern is nonspecific and overlaps substantially with that of other inflammatory and infiltrative cardiac diseases [86]. Furthermore, data on CMR strain in cardiac sarcoidosis are limited. Previously, Dabir et al. [87] reported that GLS was reduced in patients with cardiac sarcoidosis and associated with a negative outcome.

The histologic features of cardiac sarcoidosis differ according to the disease phase. The acute inflammatory phase is characterized by granulomatous infiltration, myocardial inflammation, and edema. This results in myocardial thickening, patchy increased signal intensity

on T2-weighted images, and increased T2 values [88]. Native T1 values and ECV fractions are also elevated owing to acute myocardial inflammation or edema [89]. In the chronic phase, granulomatous infiltration results in replacement scarring and wall thinning, with regional wall motion abnormalities. Native T1 values and ECV fraction can be increased due to myocardial fibrosis, and scarring [89]. Recent studies have demonstrated that native T1 and T2 values enable non-invasive recognition of cardiac involvement and activity evaluation of sarcoidosis [90]. In addition, ¹⁸F-fluorodeoxyglucose PET, which is sensitive to metabolically active inflammation, has been widely reported to play a substantial role in the diagnosis and prognosis of cardiac sarcoidosis (Fig. 8) [91].

Table 1. Cardiac MRI Characteristics for Differentiation of Thickened Myocardium Based on Histologic Features

	Hypertrophic Cardiomyopathy	Hypertensive Heart Disease	Aortic Stenosis	Anderson-Fabry Disease	Amyloidosis	Mitochondrial Cardiomyopathy	Sarcoidosis	Athlete's Heart
LVH pattern	Asymmetric > Concentric	Concentric > Asymmetric	Concentric > Asymmetric	Concentric > Asymmetric	Concentric, Asymmetric	Concentric > Asymmetric	Concentric > Asymmetric (acute)	Concentric > Asymmetric
Unique histologic features	Cardiomyocyte hypertrophy, hypertrophic nuclei, disorganized myofibrillary arrangement, interstitial fibrosis	Cardiomyocyte hypertrophy with parallel alignment, interstitial and perivascular fibrosis	Cardiomyocyte hypertrophy and interstitial fibrosis	Mild cardiomyocyte hypertrophy, perinuclear and cytoplasmic vacuoles (lysosomal glycosphingolipid accumulation)	Extracellular homogenous, eosinophilic substance deposited in interstitium	Peripheral and intermyofibrillar accumulation of abnormal mitochondria: ragged red fiber on modified Gomori trichrome stain	Noncaseating epithelioid granulomas and multinucleated giant cells in interstitium, distributed along the lymphatics	Cardiomyocyte hypertrophy without interstitial fibrosis
T1 value	↑	↑	↑	↓↓	↑↑	↑	↑	↓/↔
T2 value	↑/↔	↔	↔	↑/↔	↑	↑↑	↑ (acute)	↔
ECV fraction	↑	↑	↑	↑/↔	↑↑	↔	↑	↓
LGE	++/+/- Multifocal patchy	+/-	+/-	+/- Inferolateral	++/+ Circular subendocardial	+/-	++/+ Multifocal patchy, epicardial	Rare
LV strain on CMR	↓↓	↓/↔	↓ In severe AS	↓ Loss of base-to-apex circumferential strain gradient	↓↓ Relative apical sparing		↓	↔
Additional features	LVOT jet flow, and small LV cavity	Hypertension	AV jet flow	Systemic involvement	Atrial involvement, pericardial or pleural effusion	Hearing loss, low skeletal mass, and pericardial effusion	FDG PET (+)	Proportional cavity enlargement, improved LVH after detraining

AS = aortic valve stenosis, AV = aortic valve, CMR = cardiac magnetic resonance, ECV = extracellular volume, FDG = fluorodeoxyglucose, LGE = late gadolinium enhancement, LV = left ventricular, LVH = left ventricular hypertrophy, LVOT = left ventricular outflow tract, ↑ = mild increase, ↑↑ = moderate to marked increase, ↓ = mild decrease, ↓↓ = moderate to marked decrease, ↔ = within normal range

Athlete's Heart

Athlete's heart occurs because of cardiac adaptations to high-intensity exercise and is characterized by increased LV volume, increased LV wall thickness, increased myocardial mass, resting bradycardia, and electrocardiogram abnormalities [32,92]. SCD is fairly common in young athletes, and HCM is the most common cause of SCD among athletes. Therefore, differential diagnosis of athlete's heart from HCM is crucial but can be challenging [93].

Athlete's heart is underpinned by physiological remodeling, whereas HCM is underscored by pathological remodeling [94]. LV EDWT in athlete's heart is typically < 15 mm, and only 1.5% of athletes exhibit LV wall thickness > 15 mm [95,96]. LV wall thickening in athlete's heart is diffuse, and the chamber enlargement is proportional, as this condition is a result of physiologic wall stress and pressure [32]. In HCM, the LV end-diastolic cavity size is generally decreased and the LV end-diastolic diameter (LVEDD) is < 45 mm. In contrast, in athlete's heart, the LV cavity is enlarged and the LVEDD is > 55 mm. HCM presents as diastolic dysfunction and hyperdynamic LV systolic function, whereas diastolic dysfunction is not observed in athlete's heart [32]. Although various features can be used to differentiate athlete's heart from HCM, considerable ambiguity exists [93,97]. A recent study by Giusca et al. [98] showed that CMR-derived myocardial strain could aid in the differentiation between athlete's heart and HCM, and between athlete's heart and HHD. In contrast to HCM and HHD, the GLS of patients with athlete's heart did not differ significantly from that of the healthy participants.

Histologically, athlete's heart is characterized by increased LV mass, expansion of the cellular compartment, and smaller ECV [94], which are distinct features on CMR imaging. Abnormal focal LGE is rare in untrained individuals and athletes. Native T1 values and ECV fractions were significantly lower in athletes than in untrained individuals [99]. High-performance athletes exhibited a very low ECV fraction and increased intracellular mass index. Furthermore, a higher LV mass is correlated with a lower ECV fraction [99,100]. An increase in LV mass is associated with a reduction in ECV in athletes, but an increase in ECV in patients with HCM [100]. Thus, the absence of typical HCM features, lack of LGE, low native T1 values, and a low ECV fraction may be crucial findings in CMR imaging for differentiating athlete's heart from HCM typically showing multifocal patchy LGE, increased native T1 and T2 values,

and an increased ECV fraction.

CONCLUSIONS

An accurate differential diagnosis of LVH is mandatory to ensure appropriate treatment. The greatest strength of CMR imaging is its ability to provide various tissue contrasts and characteristics that reflect the histological changes in the myocardium. With technical innovations, CMR imaging may provide multiparametric information, including T1 and T2 values, ECV fraction, and strain data (Table 1). Although the differential diagnosis of LVH can be complex, CMR imaging enables reasonable interpretations of myocardial conditions using multiparametric analysis. This will enable the exclusion of inappropriate diagnoses and narrowing down of other potential diseases. A more precise CMR analysis based on a deeper understanding of the pathophysiological mechanisms will improve the accuracy of the differential diagnosis of LVH.

Availability of Data and Material

Data sharing does not apply to this article as no datasets were generated or analyzed during the current study.

Conflicts of Interest

Tae Hoon Kim who is on the editorial board of the *Korean Journal of Radiology* was not involved in the editorial evaluation or decision to publish this article. All remaining authors have declared no conflicts of interest.

Author Contributions

Conceptualization: Min Jae Cha, Yoon Jin Cha, Chul Hwan Park. Investigation: Cherry Kim, Chan Ho Park, Yoo Jin Hong, Jae Min Shin. Methodology: Min Jae Cha, Cherry Kim, Yoon Jin Cha, Chul Hwan Park. Project administration: Yoon Jin Cha, Chul Hwan Park. Supervision: Yoo Jin Hong, Tae Hoon Kim. Validation: Min Jae Cha, Yoon Jin Cha, Chul Hwan Park. Writing—original draft: all authors. Writing—review & editing: Min Jae Cha, Yoon Jin Cha, Yoo Jin Hong, Chul Hwan Park.

ORCID iDs

Min Jae Cha

<https://orcid.org/0000-0001-6358-8081>

Cherry Kim

<https://orcid.org/0000-0002-3361-5496>

Chan Ho Park

<https://orcid.org/0000-0002-0653-4666>

Yoo Jin Hong

<https://orcid.org/0000-0002-7276-0944>

Jae Min Shin

<https://orcid.org/0000-0003-4549-3518>

Tae Hoon Kim

<https://orcid.org/0000-0003-3598-2529>

Yoon Jin Cha

<https://orcid.org/0000-0002-5967-4064>

Chul Hwan Park

<https://orcid.org/0000-0002-0004-9475>

Funding Statement

None

Acknowledgments

The authors wish to thank Ms. Inseon Park for all artistic support related to this work.

REFERENCES

- Levy D, Anderson KM, Savage DD, Kannel WB, Christiansen JC, Castelli WP. Echocardiographically detected left ventricular hypertrophy: prevalence and risk factors. The Framingham Heart Study. *Ann Intern Med* 1988;108:7-13
- Hansen MW, Merchant N. MRI of hypertrophic cardiomyopathy: part I, MRI appearances. *AJR Am J Roentgenol* 2007;189:1335-1343
- Maron BJ, Gardin JM, Flack JM, Gidding SS, Kurosaki TT, Bild DE. Prevalence of hypertrophic cardiomyopathy in a general population of young adults. Echocardiographic analysis of 4111 subjects in the CARDIA Study. Coronary artery risk development in (young) adults. *Circulation* 1995;92:785-789
- Méndez C, Soler R, Rodríguez E, Barriales R, Ochoa JP, Monserrat L. Differential diagnosis of thickened myocardium: an illustrative MRI review. *Insights Imaging* 2018;9:695-707
- Hansen MW, Merchant N. MRI of hypertrophic cardiomyopathy: part 2, differential diagnosis, risk stratification, and posttreatment MRI appearances. *AJR Am J Roentgenol* 2007;189:1344-1352
- Lorell BH, Carabello BA. Left ventricular hypertrophy: pathogenesis, detection, and prognosis. *Circulation* 2000;102:470-479
- Giesbrandt KJ, Bolan CW, Shapiro BP, Edwards WD, Mergo PJ. Diffuse diseases of the myocardium: MRI-pathologic review of nondilated cardiomyopathies. *AJR Am J Roentgenol* 2013;200:W266-W273
- Varma PK, Neema PK. Hypertrophic cardiomyopathy: part 1 - introduction, pathology and pathophysiology. *Ann Card Anaesth* 2014;17:118-124
- Saremi F, Sánchez-Quintana D, Mori S, Muresian H, Spicer DE, Hassani C, et al. Fibrous skeleton of the heart: anatomic overview and evaluation of pathologic conditions with CT and MR imaging. *Radiographics* 2017;37:1330-1351
- Maron BJ. Hypertrophic cardiomyopathy: a systematic review. *JAMA* 2002;287:1308-1320
- O'Hanlon R, Pennell DJ. Cardiovascular magnetic resonance in the evaluation of hypertrophic and infiltrative cardiomyopathies. *Heart Fail Clin* 2009;5:369-387, vi
- Semsarian C, Ingles J, Maron MS, Maron BJ. New perspectives on the prevalence of hypertrophic cardiomyopathy. *J Am Coll Cardiol* 2015;65:1249-1254
- Klues HG, Schiffers A, Maron BJ. Phenotypic spectrum and patterns of left ventricular hypertrophy in hypertrophic cardiomyopathy: morphologic observations and significance as assessed by two-dimensional echocardiography in 600 patients. *J Am Coll Cardiol* 1995;26:1699-1708
- Nourelidin RA, Liu S, Nacif MS, Judge DP, Halushka MK, Abraham TP, et al. The diagnosis of hypertrophic cardiomyopathy by cardiovascular magnetic resonance. *J Cardiovasc Magn Reson* 2012;14:17
- O'Hanlon R, Assomull RG, Prasad SK. Use of cardiovascular magnetic resonance for diagnosis and management in hypertrophic cardiomyopathy. *Curr Cardiol Rep* 2007;9:51-56
- Baxi AJ, Restrepo CS, Vargas D, Marmol-Velez A, Ocazonez D, Murillo H. Hypertrophic cardiomyopathy from A to Z: genetics, pathophysiology, imaging, and management. *Radiographics* 2016;36:335-354
- Elliott PM, Anastasakis A, Borger MA, Borggrefe M, Cecchi F, Charron P, et al. 2014 ESC Guidelines on diagnosis and management of hypertrophic cardiomyopathy: the Task Force for the Diagnosis and Management of Hypertrophic Cardiomyopathy of the European Society of Cardiology (ESC). *Eur Heart J* 2014;35:2733-2779
- Burrage MK, Ferreira VM. Cardiovascular magnetic resonance for the differentiation of left ventricular hypertrophy. *Curr Heart Fail Rep* 2020;17:192-204
- Quarta G, Aquaro GD, Pedrotti P, Pontone G, Dellegrottaglie S, Iacovoni A, et al. Cardiovascular magnetic resonance imaging in hypertrophic cardiomyopathy: the importance of clinical context. *Eur Heart J Cardiovasc Imaging* 2018;19:601-610
- Bruder O, Wagner A, Jensen CJ, Schneider S, Ong P, Kispert EM, et al. Myocardial scar visualized by cardiovascular magnetic resonance imaging predicts major adverse events in patients with hypertrophic cardiomyopathy. *J Am Coll Cardiol* 2010;56:875-887
- Mentias A, Raeisi-Giglou P, Smedira NG, Feng K, Sato K, Wazni O, et al. Late gadolinium enhancement in patients with hypertrophic cardiomyopathy and preserved systolic function. *J Am Coll Cardiol* 2018;72:857-870
- Mewton N, Liu CY, Croisille P, Bluemke D, Lima JA. Assessment of myocardial fibrosis with cardiovascular magnetic resonance. *J Am Coll Cardiol* 2011;57:891-903
- Hinojar R, Varma N, Child N, Goodman B, Jabbour A, Yu CY, et al. T1 mapping in discrimination of hypertrophic

- phenotypes: hypertensive heart disease and hypertrophic cardiomyopathy: findings from the international T1 multicenter cardiovascular magnetic resonance study. *Circ Cardiovasc Imaging* 2015;8:e003285
24. Axelsson Raja A, Farhad H, Valente AM, Couce JP, Jefferies JL, Bundgaard H, et al. Prevalence and progression of late gadolinium enhancement in children and adolescents with hypertrophic cardiomyopathy. *Circulation* 2018;138:782-792
 25. Xu J, Zhuang B, Sirajuddin A, Li S, Huang J, Yin G, et al. MRI T1 mapping in hypertrophic cardiomyopathy: evaluation in patients without late gadolinium enhancement and hemodynamic obstruction. *Radiology* 2020;294:275-286
 26. Huang L, Ran L, Zhao P, Tang D, Han R, Ai T, et al. MRI native T1 and T2 mapping of myocardial segments in hypertrophic cardiomyopathy: tissue remodeling manifested prior to structure changes. *Br J Radiol* 2019;92:20190634
 27. Gommans DHF, Cramer GE, Bakker J, Dieker HJ, Michels M, Fouraux MA, et al. High T2-weighted signal intensity for risk prediction of sudden cardiac death in hypertrophic cardiomyopathy. *Int J Cardiovasc Imaging* 2018;34:113-120
 28. Neisius U, Myerson L, Fahmy AS, Nakamori S, El-Rewaidy H, Joshi G, et al. Cardiovascular magnetic resonance feature tracking strain analysis for discrimination between hypertensive heart disease and hypertrophic cardiomyopathy. *PLoS One* 2019;14:e0221061
 29. Rodrigues JC, Rohan S, Ghosh Dastidar A, Harries I, Lawton CB, Ratcliffe LE, et al. Hypertensive heart disease versus hypertrophic cardiomyopathy: multi-parametric cardiovascular magnetic resonance discriminators when end-diastolic wall thickness ≥ 15 mm. *Eur Radiol* 2017;27:1125-1135
 30. Sipola P, Magga J, Husso M, Jääskeläinen P, Peuhkurinen K, Kuusisto J. Cardiac MRI assessed left ventricular hypertrophy in differentiating hypertensive heart disease from hypertrophic cardiomyopathy attributable to a sarcomeric gene mutation. *Eur Radiol* 2011;21:1383-1389
 31. Maceira AM, Mohiaddin RH. Cardiovascular magnetic resonance in systemic hypertension. *J Cardiovasc Magn Reson* 2012;14:28
 32. Carbone A, D'Andrea A, Riegler L, Scarafilo R, Pezzullo E, Martone F, et al. Cardiac damage in athlete's heart: when the "supernormal" heart fails! *World J Cardiol* 2017;9:470-480
 33. Rudolph A, Abdel-Aty H, Bohl S, Boyé P, Zagrosek A, Dietz R, et al. Noninvasive detection of fibrosis applying contrast-enhanced cardiac magnetic resonance in different forms of left ventricular hypertrophy relation to remodeling. *J Am Coll Cardiol* 2009;53:284-291
 34. Puntmann VO, Jahnke C, Gebker R, Schnackenburg B, Fox KF, Fleck E, et al. Usefulness of magnetic resonance imaging to distinguish hypertensive and hypertrophic cardiomyopathy. *Am J Cardiol* 2010;106:1016-1022
 35. Wu LM, Wu R, Ou YR, Chen BH, Yao QY, Lu Q, et al. Fibrosis quantification in hypertensive heart disease with LVH and non-LVH: findings from T1 mapping and contrast-free cardiac diffusion-weighted imaging. *Sci Rep* 2017;7:559
 36. Kato TS, Noda A, Izawa H, Yamada A, Obata K, Nagata K, et al. Discrimination of nonobstructive hypertrophic cardiomyopathy from hypertensive left ventricular hypertrophy on the basis of strain rate imaging by tissue Doppler ultrasonography. *Circulation* 2004;110:3808-3814
 37. Nkomo VT, Gardin JM, Skelton TN, Gottdiener JS, Scott CG, Enriquez-Sarano M. Burden of valvular heart diseases: a population-based study. *Lancet* 2006;368:1005-1011
 38. Hein S, Arnon E, Kostin S, Schönburg M, Elsässer A, Polyakova V, et al. Progression from compensated hypertrophy to failure in the pressure-overloaded human heart: structural deterioration and compensatory mechanisms. *Circulation* 2003;107:984-991
 39. Dweck MR, Joshi S, Murigu T, Gulati A, Alpendurada F, Jabbour A, et al. Left ventricular remodeling and hypertrophy in patients with aortic stenosis: insights from cardiovascular magnetic resonance. *J Cardiovasc Magn Reson* 2012;14:50
 40. Grossman W. Cardiac hypertrophy: useful adaptation or pathologic process? *Am J Med* 1980;69:576-584
 41. Debry N, Maréchaux S, Rusinaru D, Peltier M, Messika-Zeitoun D, Menet A, et al. Prognostic significance of left ventricular concentric remodelling in patients with aortic stenosis. *Arch Cardiovasc Dis* 2017;110:26-34
 42. Dweck MR, Joshi S, Murigu T, Alpendurada F, Jabbour A, Melina G, et al. Midwall fibrosis is an independent predictor of mortality in patients with aortic stenosis. *J Am Coll Cardiol* 2011;58:1271-1279
 43. Krayenbuehl HP, Hess OM, Monrad ES, Schneider J, Moll G, Turina M. Left ventricular myocardial structure in aortic valve disease before, intermediate, and late after aortic valve replacement. *Circulation* 1989;79:744-755
 44. Singh A, Horsfield MA, Bekele S, Khan JN, Greiser A, McCann GP. Myocardial T1 and extracellular volume fraction measurement in asymptomatic patients with aortic stenosis: reproducibility and comparison with age-matched controls. *Eur Heart J Cardiovasc Imaging* 2015;16:763-770
 45. Treibel TA, Kozor R, Schofield R, Benedetti G, Fontana M, Bhuvana AN, et al. Reverse myocardial remodeling following valve replacement in patients with aortic stenosis. *J Am Coll Cardiol* 2018;71:860-871
 46. Everett RJ, Treibel TA, Fukui M, Lee H, Rigolli M, Singh A, et al. Extracellular myocardial volume in patients with aortic stenosis. *J Am Coll Cardiol* 2020;75:304-316
 47. Park SJ, Cho SW, Kim SM, Ahn J, Carriere K, Jeong DS, et al. Assessment of myocardial fibrosis using multimodality imaging in severe aortic stenosis: comparison with histologic fibrosis. *JACC Cardiovasc Imaging* 2019;12:109-119
 48. Hwang JW, Kim SM, Park SJ, Cho EJ, Kim EK, Chang SA, et al. Assessment of reverse remodeling predicted by myocardial deformation on tissue tracking in patients with

- severe aortic stenosis: a cardiovascular magnetic resonance imaging study. *J Cardiovasc Magn Reson* 2017;19:80
49. Musa TA, Uddin A, Swoboda PP, Fairbairn TA, Dobson LE, Singh A, et al. Cardiovascular magnetic resonance evaluation of symptomatic severe aortic stenosis: association of circumferential myocardial strain and mortality. *J Cardiovasc Magn Reson* 2017;19:13
 50. Kim MY, Park EA, Lee W, Lee SP. Cardiac magnetic resonance feature tracking in aortic stenosis: exploration of strain parameters and prognostic value in asymptomatic patients with preserved ejection fraction. *Korean J Radiol* 2020;21:268-279
 51. Yogasundaram H, Kim D, Oudit O, Thompson RB, Weidemann F, Oudit GY. Clinical features, diagnosis, and management of patients with Anderson-Fabry cardiomyopathy. *Can J Cardiol* 2017;33:883-897
 52. El-Abassi R, Singhal D, England JD. Fabry's disease. *J Neurol Sci* 2014;344:5-19
 53. Zarate YA, Hopkin RJ. Fabry's disease. *Lancet* 2008;372:1427-1435
 54. Wu JC, Ho CY, Skali H, Abichandani R, Wilcox WR, Banikazemi M, et al. Cardiovascular manifestations of Fabry disease: relationships between left ventricular hypertrophy, disease severity, and alpha-galactosidase A activity. *Eur Heart J* 2010;31:1088-1097
 55. Mathur S, Dreisbach JG, Karur GR, Iwanochko RM, Morel CF, Wasim S, et al. Loss of base-to-apex circumferential strain gradient assessed by cardiovascular magnetic resonance in Fabry disease: relationship to T1 mapping, late gadolinium enhancement and hypertrophy. *J Cardiovasc Magn Reson* 2019;21:45
 56. Moon JC, Sachdev B, Elkington AG, McKenna WJ, Mehta A, Pennell DJ, et al. Gadolinium enhanced cardiovascular magnetic resonance in Anderson-Fabry disease. Evidence for a disease specific abnormality of the myocardial interstitium. *Eur Heart J* 2003;24:2151-2155
 57. Karur GR, Robison S, Iwanochko RM, Morel CF, Crean AM, Thavendiranathan P, et al. Use of myocardial T1 mapping at 3.0 T to differentiate Anderson-Fabry disease from hypertrophic cardiomyopathy. *Radiology* 2018;288:398-406
 58. Pica S, Sado DM, Maestrini V, Fontana M, White SK, Treibel T, et al. Reproducibility of native myocardial T1 mapping in the assessment of Fabry disease and its role in early detection of cardiac involvement by cardiovascular magnetic resonance. *J Cardiovasc Magn Reson* 2014;16:99
 59. Sado DM, White SK, Piechnik SK, Banyersad SM, Treibel T, Captur G, et al. Identification and assessment of Anderson-Fabry disease by cardiovascular magnetic resonance noncontrast myocardial T1 mapping. *Circ Cardiovasc Imaging* 2013;6:392-398
 60. Camporeale A, Pieroni M, Pieruzzi F, Lusardi P, Pica S, Spada M, et al. Predictors of clinical evolution in prehypertrophic Fabry disease. *Circ Cardiovasc Imaging* 2019;12:e008424
 61. Weidemann F, Niemann M, Störk S, Breunig F, Beer M, Sommer C, et al. Long-term outcome of enzyme-replacement therapy in advanced Fabry disease: evidence for disease progression towards serious complications. *J Intern Med* 2013;274:331-341
 62. Nordin S, Kozor R, Medina-Menacho K, Abdel-Gadir A, Baig S, Sado DM, et al. Proposed stages of myocardial phenotype development in Fabry disease. *JACC Cardiovasc Imaging* 2019;12:1673-1683
 63. Banyersad SM, Moon JC, Whelan C, Hawkins PN, Wechalekar AD. Updates in cardiac amyloidosis: a review. *J Am Heart Assoc* 2012;1:e000364
 64. Fontana M, Banyersad SM, Treibel TA, Abdel-Gadir A, Maestrini V, Lane T, et al. Differential myocyte responses in patients with cardiac transthyretin amyloidosis and light-chain amyloidosis: a cardiac MR imaging study. *Radiology* 2015;277:388-397
 65. Oda S, Kidoh M, Nagayama Y, Takashio S, Usuku H, Ueda M, et al. Trends in diagnostic imaging of cardiac amyloidosis: emerging knowledge and concepts. *Radiographics* 2020;40:961-981
 66. Izumiya Y, Takashio S, Oda S, Yamashita Y, Tsujita K. Recent advances in diagnosis and treatment of cardiac amyloidosis. *J Cardiol* 2018;71:135-143
 67. Maleszewski JJ. Cardiac amyloidosis: pathology, nomenclature, and typing. *Cardiovasc Pathol* 2015;24:343-350
 68. Philippakis AA, Falk RH. Cardiac amyloidosis mimicking hypertrophic cardiomyopathy with obstruction: treatment with disopyramide. *Circulation* 2012;125:1821-1824
 69. Pozo E, Kanwar A, Deochand R, Castellano JM, Naib T, Pazos-López P, et al. Cardiac magnetic resonance evaluation of left ventricular remodelling distribution in cardiac amyloidosis. *Heart* 2014;100:1688-1695
 70. Martinez-Naharro A, Treibel TA, Abdel-Gadir A, Bulluck H, Zumbo G, Knight DS, et al. Magnetic resonance in transthyretin cardiac amyloidosis. *J Am Coll Cardiol* 2017;70:466-477
 71. Fattori R, Rocchi G, Celletti F, Bertaccini P, Rapezzi C, Gavelli G. Contribution of magnetic resonance imaging in the differential diagnosis of cardiac amyloidosis and symmetric hypertrophic cardiomyopathy. *Am Heart J* 1998;136:824-830
 72. Kim JY, Hong YJ, Han K, Lee HJ, Hur J, Kim YJ, et al. Regional amyloid burden differences evaluated using quantitative cardiac MRI in patients with cardiac amyloidosis. *Korean J Radiol* 2021;22:880-889
 73. Haaf P, Garg P, Messroghli DR, Broadbent DA, Greenwood JP, Plein S. Cardiac T1 mapping and extracellular volume (ECV) in clinical practice: a comprehensive review. *J Cardiovasc Magn Reson* 2016;18:89
 74. Gillmore JD, Maurer MS, Falk RH, Merlini G, Damy T, Dispenzieri A, et al. Nonbiopsy diagnosis of cardiac transthyretin amyloidosis. *Circulation* 2016;133:2404-2412
 75. Ruberg FL, Miller EJ. Nuclear tracers for transthyretin cardiac amyloidosis: time to bone up? *Circ Cardiovasc Imaging*

- 2013;6:162-164
76. Florian A, Ludwig A, Stubbe-Dräger B, Boentert M, Young P, Waltenberger J, et al. Characteristic cardiac phenotypes are detected by cardiovascular magnetic resonance in patients with different clinical phenotypes and genotypes of mitochondrial myopathy. *J Cardiovasc Magn Reson* 2015;17:40
 77. Dimmock DP, Lawlor MW. Presentation and diagnostic evaluation of mitochondrial disease. *Pediatr Clin North Am* 2017;64:161-171
 78. Kuno T, Imaeda S, Asakawa Y, Nakamura H, Takemura G, Asahara D, et al. Mitochondrial cardiomyopathy presenting as dilated phase of hypertrophic cardiomyopathy diagnosed with histological and genetic analyses. *Case Rep Cardiol* 2017;2017:9473917
 79. Partington SL, Givertz MM, Gupta S, Kwong RY. Cardiac magnetic resonance aids in the diagnosis of mitochondrial cardiomyopathy. *Circulation* 2011;123:e227-e229
 80. Nakanishi M, Harada M, Tadamura E, Kotani H, Kawakami R, Kuwahara K, et al. Images in cardiovascular medicine. Mitochondrial cardiomyopathy evaluated with cardiac magnetic resonance. *Circulation* 2007;116:e25-e26
 81. Dubrey SW, Falk RH. Diagnosis and management of cardiac sarcoidosis. *Prog Cardiovasc Dis* 2010;52:336-346
 82. Iwai K, Tachibana T, Takemura T, Matsui Y, Kitaichi M, Kawabata Y. Pathological studies on sarcoidosis autopsy. I. Epidemiological features of 320 cases in Japan. *Acta Pathol Jpn* 1993;43:372-376
 83. Birnie DH, Nery PB, Ha AC, Beanlands RS. Cardiac sarcoidosis. *J Am Coll Cardiol* 2016;68:411-421
 84. Sadek MM, Yung D, Birnie DH, Beanlands RS, Nery PB. Corticosteroid therapy for cardiac sarcoidosis: a systematic review. *Can J Cardiol* 2013;29:1034-1041
 85. Birnie DH, Sauer WH, Bogun F, Cooper JM, Culver DA, Duvernoy CS, et al. HRS expert consensus statement on the diagnosis and management of arrhythmias associated with cardiac sarcoidosis. *Heart Rhythm* 2014;11:1305-1323
 86. Jeudy J, Burke AP, White CS, Kramer GB, Frazier AA. Cardiac sarcoidosis: the challenge of radiologic-pathologic correlation: from the radiologic pathology archives. *Radiographics* 2015;35:657-679
 87. Dabir D, Meyer D, Kuetting D, Luetkens J, Homs R, Pizarro C, et al. Diagnostic value of cardiac magnetic resonance strain analysis for detection of cardiac sarcoidosis. *Rofa* 2018;190:712-721
 88. Vignaux O, Dhote R, Duboc D, Blanche P, Devaux JY, Weber S, et al. Detection of myocardial involvement in patients with sarcoidosis applying T2-weighted, contrast-enhanced, and cine magnetic resonance imaging: initial results of a prospective study. *J Comput Assist Tomogr* 2002;26:762-767
 89. Greulich S, Kitterer D, Latus J, Agur E, Steubing H, Kaesemann P, et al. Comprehensive cardiovascular magnetic resonance assessment in patients with sarcoidosis and preserved left ventricular ejection fraction. *Circ Cardiovasc Imaging* 2016;9:e005022
 90. Puntmann VO, Isted A, Hinojar R, Foote L, Carr-White G, Nagel E. T1 and T2 mapping in recognition of early cardiac involvement in systemic sarcoidosis. *Radiology* 2017;285:63-72
 91. Youssef G, Leung E, Mylonas I, Nery P, Williams K, Wisenberg G, et al. The use of 18F-FDG PET in the diagnosis of cardiac sarcoidosis: a systematic review and metaanalysis including the Ontario experience. *J Nucl Med* 2012;53:241-248
 92. Pluim BM, Zwinderman AH, van der Laarse A, van der Wall EE. The athlete's heart. A meta-analysis of cardiac structure and function. *Circulation* 2000;101:336-344
 93. Maron BJ, Pelliccia A. The heart of trained athletes: cardiac remodeling and the risks of sports, including sudden death. *Circulation* 2006;114:1633-1644
 94. Bernardo BC, Weeks KL, Pretorius L, McMullen JR. Molecular distinction between physiological and pathological cardiac hypertrophy: experimental findings and therapeutic strategies. *Pharmacol Ther* 2010;128:191-227
 95. Basavarajaiah S, Wilson M, Whyte G, Shah A, McKenna W, Sharma S. Prevalence of hypertrophic cardiomyopathy in highly trained athletes: relevance to pre-participation screening. *J Am Coll Cardiol* 2008;51:1033-1039
 96. Scharhag J, Schneider G, Urhausen A, Rochette V, Kramann B, Kindermann W. Athlete's heart: right and left ventricular mass and function in male endurance athletes and untrained individuals determined by magnetic resonance imaging. *J Am Coll Cardiol* 2002;40:1856-1863
 97. Lauschke J, Maisch B. Athlete's heart or hypertrophic cardiomyopathy? *Clin Res Cardiol* 2009;98:80-88
 98. Giusca S, Steen H, Montenbruck M, Patel AR, Pieske B, Erley J, et al. Multi-parametric assessment of left ventricular hypertrophy using late gadolinium enhancement, T1 mapping and strain-encoded cardiovascular magnetic resonance. *J Cardiovasc Magn Reson* 2021;23:92
 99. McDiarmid AK, Swoboda PP, Erhayiem B, Lancaster RE, Lyall GK, Broadbent DA, et al. Athletic cardiac adaptation in males is a consequence of elevated myocyte mass. *Circ Cardiovasc Imaging* 2016;9:e003579
 100. Swoboda PP, McDiarmid AK, Erhayiem B, Broadbent DA, Dobson LE, Garg P, et al. Assessing myocardial extracellular volume by T1 mapping to distinguish hypertrophic cardiomyopathy from athlete's heart. *J Am Coll Cardiol* 2016;67:2189-2190